Influence of the Guard Rings on the Response of SSD-Based Radiation Monitors in Space Environment: Applications to ICARE Monitors

Pablo Caron, Maxime Pinson, Sébastien Bourdarie, Didier Falguère, Bastien Taponat, Philippe Bourdoux, Jérôme Carron, Maxime Ruffenach, Robert Ecoffet

Influence of the Guard Rings on the response of SSD-based radiation monitors in space environment: applications to ICARE monitors

P. Caron[1], M. Pinson[1], S. Bourdarie[1], D. Falguère[1], B. Taponat[2], P. Bourdoux[2], J. Carron[3], M. Ruffenach[3], R. Ecoffet[3]

***Abstract*— The aim of this work is to analyze the influence of the guard rings (GRs) in solid state detectors (SSDs). Depending on the applied potential, the collection of charges can be disturbed. A study on SSDs with floating and grounded GRs is conducted. The tools needed to do so are presented (GEANT4, Sentaurus and Garfield++). Experimental measurements have been performed on Micron Semiconductor Ltd SSDs which are composed of multiple guard rings (MGRs). Finally, a first application on the ICARE_NG² (Influence sur les Composants Avancés des Radiations de l'Espace) radiation monitor is proposed with a comparison of the response functions (RFs) according to the potential applied on the GRs. Improved performances are observed when the GRs are grounded. A second application on the ICARE_NG currently embedded on Eutelsat 7C (E7C) is also proposed by using the GRs as active shielding, allowing improvements in the measurement of high energy particles.**

***Index Terms*— Space environment, particle fluxes, electron, proton, EOR, GEO, Guard Rings, SSDs**

I. Introduction

Radiation monitors are essential to improve our knowledge of the radiation belts : they allow in-situ measurements of the particle fluxes. There are several kinds of radiation monitors: some based on scintillators [1], Solid State Detectors (SSDs) [2]–[4], some using magnets [5].

SSD-based detectors, as used in ICARE (Influence sur les Composants Avancés des Radiations de l'Espace) [4], [6], [7], are based on PN junctions operated in reverse bias. The substrate is typically n-type high resistivity silicon. When a particle crosses the detector, it will interact with the electrons and nuclei of the medium and lose energy. During these interactions, electron-hole pairs are created and are referred to as carriers. As there is an electric field induced by the bias voltage applied between the electrodes, the carriers will migrate towards them. The motion of the carriers generates a current, which is measured and processed to deduce the deposited energy.

Important efforts have been carried out in the development of PN junction based SSD detectors that minimize leakage current while optimizing IV characteristics [8]. Such designs focus on reducing the maximum value of a local electric field, which appears near the border of the PN junction and can lead to impact ionization and avalanche breakdown. There are several methods to do this and the use of guard rings (GR) or multiple guard rings (MGR) is commonly proposed in the literature [9]. This approach redistributes the potential around a junction over a wide area covered by MGR.

This paper aims to illustrate the influence of the GR (depending on the applied potential) on the response function (RF) of a radiation monitor. Applications on the ICARE_NG and ICARE_NG² monitors are detailed in the last parts of the paper.

II. SSD-based radiation monitor

A. Response function

Typically, a radiation monitor samples the energy deposited in an SSD through a dedicated charge amplifier and pulse shaper.

Then, the transformation of deposited energy to incident energy is done by post-processing, using the RF of the instrument. Fig. 1 presents the proton RF of the PE1 detection head of ICARE_NG, onboard the E7C satellite. In addition to the geometry of the detection head, the geometry of the satellite is also taken into account in the construction of this RF. The color scale gives the geometric factor (GEF), in other words, the proton sensitivity of the detection head. The name PE1 indicates that this detection head can measure proton and electron fluxes and uses only one SSD.

The radiation monitor continuously builds-up a histogram whose bins correspond to deposited energy values and then, by inversion or other techniques, it is possible to reconstruct the associated fluxes. The general expression that relates the counts (histograms) to fluxes is given in (1).

$$C = \sum_{n=p,e} \int_0^\infty f_{n\,\mathrm{diff}}(E)\,\mathrm{RF_n}(E)\,dE \qquad (1)$$

Manuscript received November 14, 2022; This work was supported by Grants 4500070858, which part of CNES R&T program.

P. Caron, M. Pinson, S. Bourdarie and D. Falguère are with ONERA/DPHY, Université de Toulouse, Toulouse, France (email: Pablo.Caron@onera.fr)

B. Taponat and P. Bourdoux are with the EREMS Society, Flourens, France (email: Philippe.Bourdoux@erems.fr)

M. Ruffenach, R. Ecoffet and J. Carron are with CNES, The French Space Agency, Toulouse, France (email: Robert.Ecoffet@cnes.fr)

With C, the counts, RF, the response function (as in Fig. 1) and f_{diff}, the differential flux (the physical quantity of interest). p and e represent respectively proton and electron incident particles with the energy E.

Generally, the design of a radiation monitor is made to have a greater sensitivity for a single species and/or a greater sensitivity for an energy or a range of energies.

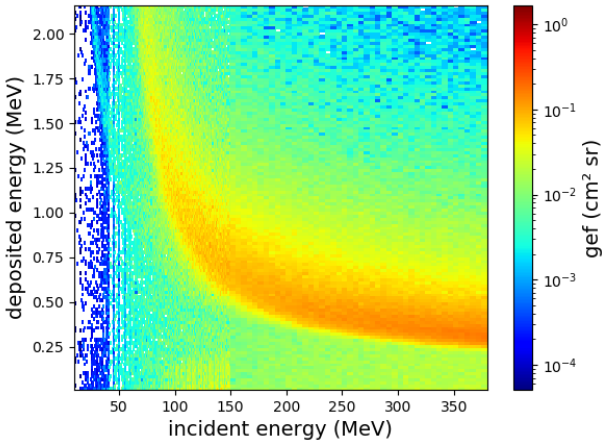

Fig. 1. Typical example of an ICARE_NG response function under isotropic proton environment, onboard the E7C satellite.

III. Solid State Detector: Physical Concept and Measurements

A. Description

SSDs are the sensitive regions in a radiation monitor. As previously mentioned, the passage of a particle inside an SSD causes a cascade of electron-hole pairs, which are then collected by the system's electrodes. In order to optimize this collection of charges (avoiding recombination effects), the system is reverse-biased.

Fig. 2 gives a cross section of an SSD with only one GR. The main electrodes (assimilated to an anode and cathode) are placed on the p+ and n+ regions. Additional electrodes are located on GRs.

The junction side is assimilated to a p+ region while the ohmic side is assimilated to an n+ region.

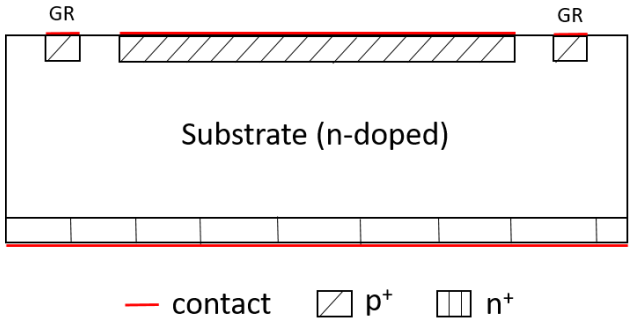

Fig. 2. 2D schematic representation of an SSD with one GR

There are several papers in the literature discussing the performance (e.g., by improving breakdown voltage, reducing leakage current) of SSDs as a function of GRs [9]. However, these GRs may influence the collection of charges [10]. The impact of the GRs on the monitor's radiation responses, depending on the type of connection used (grounded or floating) and the associated dimensions and spacing is examined in this paper.

B. Charge collection induced by GRs

Tests were performed on a Micron SSD whose characteristics are given in Table I.

TABLE I
SSD PARAMETERS

Manufacturer	diameter	thickness	Depletion voltage
Micron	16 mm	1000 µm	110 V

Wires were connected to the GRs, to the junction face, and to the ohmic side.

Energy deposition measurements have been performed with a radioactive source consisting of three elements: Am^{241} (Americium), Pu^{239} (Plutonium) and Cm^{244} (Curium). These isotopes are associated to three alpha particle energies: 5.1 MeV, 5.4 MeV and 5.8 MeV. The set-up used is illustrated in Fig. 3.

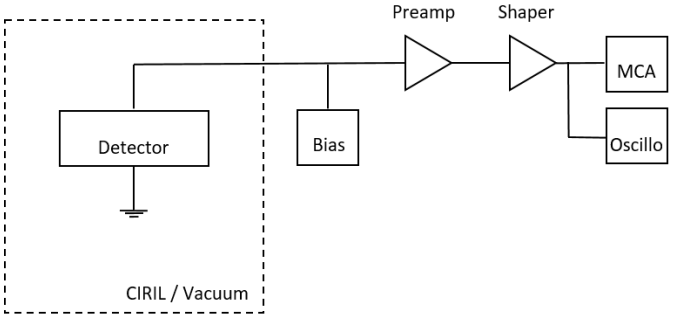

Fig. 3. Diagram of the set-up used to measure deposited energy in the SSD

The SSD was, therefore, placed in the CIRIL chamber, under vacuum. The junction side is directly exposed to the source, in order to observe the effect of the GRs.

Two measurements were performed, one by grounding the guard rings and a second by floating them. The results obtained by fixing the guard rings to the ground are presented in Fig. 4. Three peaks associated with the three elements of the radioactive source can be clearly identified.

Fig. 5 presents our results when the guard rings are floating. The presence of secondary peaks can be observed, which are not related to the radioactive source used. This is a direct effect of the influence of the guard rings in the collection of charges when these guard rings are floating.

With particles with small ranges (less than the depth of the SSD), this effect is only observed on the face where the guard rings are placed (junction side). Thus, no secondary peaks are

observed when irradiating the ohmic side. However, we can expect to observe an effect if the range of the particle becomes of the order of or greater than the depth of the diode.

The way to simulate the influence of the GRs is presented in the next sections with two objectives:

- Quantify the impact of GRs on the performance of a radiation monitor when these guard rings are floating
- Increase the performance of the radiation monitor by using these guard rings

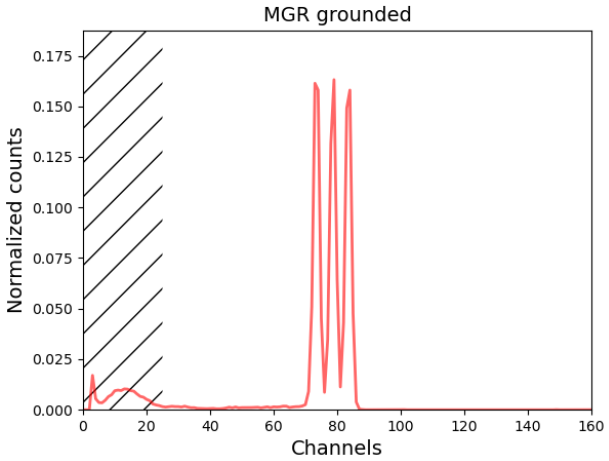

Fig. 4. Histogram of deposited energies extracted from the MCA (Multichannel Analyzer) when the GRs are grounded. The dashed part corresponds to the noise level of the set-up.

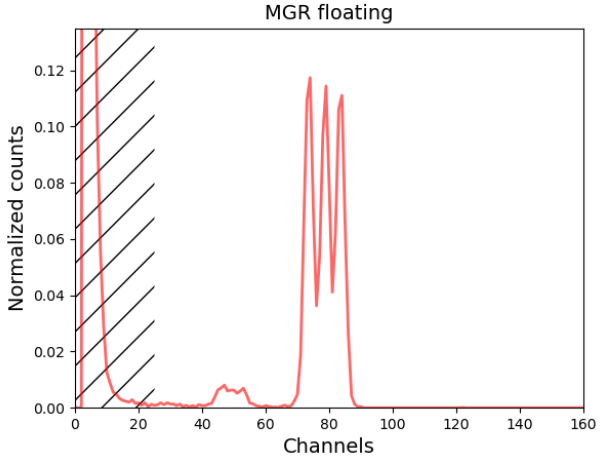

Fig. 5. Histogram of deposited energies extracted from the MCA (Multichannel Analyzer) when the GRs are floating. The dashed part corresponds to the noise level of the set-up.

IV. Simulation Chain

Simulating the response of the instrument in electron and proton environments until the charges are collected at the electrodes involves several calculation steps.

Indeed, it is necessary to simulate the electric field of the SSD, the cascade of electron-hole pairs generated by the incident particle in the SSD and the diffusion of these electron-hole pairs in the electric field.

For this, three tools have been used together and a brief presentation of each of them is now provided.

A. *GEANT4*

GEANT4 is a C++ framework for the simulation of the passage of particles through matter [11]–[13]. During simulations, version 10.5 was used and electromagnetic processes were managed using PhysListEmStandardNR physics list. All ionizing energies released into the medium are sampled.

B. *Garfield++*

Garfield++ [14] is a C++-based simulation tool to manage the drift of the charges to the electrodes of a device.
Based on deposited ionizing energy simulated by GEANT4, the average energy to create an electron-hole pair ($W_{Si} \sim 3.6$ eV) and the Fano factor ($F_{Si} \sim 0.11$), the number of charges is estimated.

The signals calculated with Garfield++ are deduced from the Shockley-Ramo theorem [15], [16]. The current $i(t)$ induced by a charge q at a position $\vec{r}$ moving at a velocity $\vec{v}$ is given by Eq. (1) [17]:

$$i(t) = -q \cdot \vec{v} \cdot \vec{E}_w(\vec{r}) \quad (2)$$

Where $\vec{E}_w$ is the so-called weighting field associated to the electrode to be read out.

Garfield++ does not solve the semiconductor equations but accepts two- and three-dimensional field maps computed by several external programs as a basis for its calculations [18]. In this paper, such maps have been simulated thanks to Synopsys/Sentaurus [19].

C. *Synopsys/Sentaurus*

The Synopsys Sentaurus TCAD™ software [19] is used to calculate electric fields in the detectors. This software program is widely used for semiconductor devices simulation. Sentaurus TCAD™ offers a vast set of physical models to analyze semiconductor structures and solves semiconductor equations in user-defined geometries. From the doping levels and the voltages applied to the electrodes, it is thus possible to evaluate several quantities such as the electric field of the system.

Several technological parameters have to be evaluated beforehand such as the doping of the substrate and the p+, n+, and GR regions.

The calculation of the weighting field $\vec{E}_w$, as required by Garfield++, is not immediate and involves two steps:

- The first one corresponds to a simulation in the nominal conditions of our device.
- The second imposes a slight increase in the voltage applied to the electrode to be read out compared to its nominal state.

V. Numerical Simulations

The simulated SSD had a depth of 300 µm, a radius of 1.5 mm and, three guard rings. The parameters (dimensions and

spacing) of the first three guard rings of the Micron SSD were used. A scan of the main junction with 30 MeV protons incoming perpendicularly has been performed. The following subsections observe the behavior of the sensitive volume of SSDs as a function of the connections applied to the GRs (grounded and floating).

A. GRs grounded

Fig. 6 presents the case where the GRs are grounded. This configuration creates a sensitive volume with the same width as the junction side.

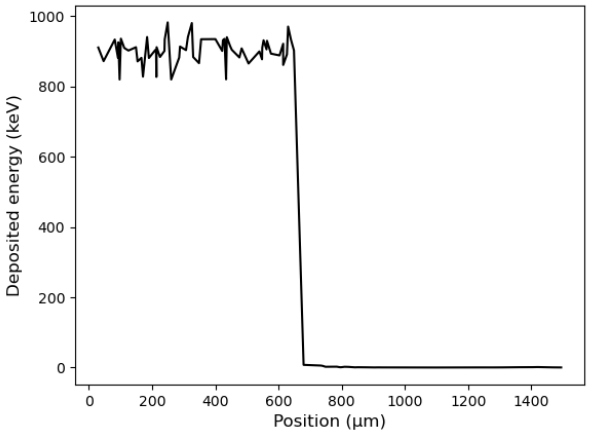

Fig. 6. Deposited energy as a function of impact position for 30 MeV proton irradiation. The GRs are grounded.

B. GRs floating

Fig. 7 presents the case where the GRs are floating.

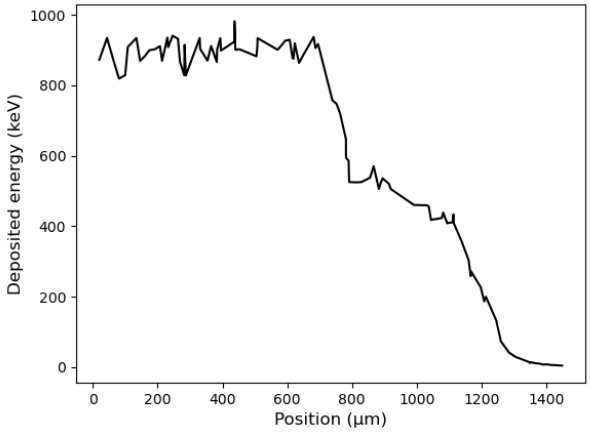

Fig. 7. Deposited energy as a function of impact position for 30 MeV proton irradiation. The GRs are floating.

As shown in Fig. 7, in addition to an increase of the sensitive volume (compared to the "GR-grounded" configuration), floating GRs cause new regimes of charge collections (as experimentally observed).

The effective dimension of the sensitive volume and the different collection stages depend entirely on the dimensions, the spacing and the number of GRs.

Considering the discussion in Section II.A, creating intermediate stages in the charge collections potentially degrades the response function of the instrument by increasing the low-deposited energy events.

Of course, in a controlled radiative environment, these effects can be avoided by ensuring that only the center of the SSD is irradiated. In addition, when several SSDs are stacked and the instrument only operates in coincidence mode, this effect can also be minimized.

VI. Response functions with grounded or floating GRs

Simulations have been performed with a realistic detection head, using the geometry of the PE1 head of ICARE_NG² (see Fig. 8).

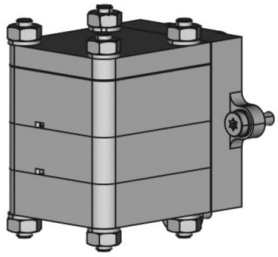

Fig. 8. PE1 detection head of ICARE_NG²

PE1 is composed of a single SSD. The new generation of ICARE_NG is onboard the Hotbird 13F and 13G satellites. The major difference between ICARE_NG and ICARE_NG² is the development of a detection head dedicated to measure low proton energies.

The precise structure of the guard rings provided by Micron has been implemented. In order to simulate the radiative environment of the radiation belts, an isotropic source has been used.

The objective here is to quantify from an operational point of view the impact of the guard rings on the performance of a radiation monitor. These performances correspond, in our case, to the capacity of the monitor to measure a wide range in energy.

To do this, simulations in proton environment have been performed and the ratio of the RFs is presented in Fig. 9.

As already discussed, the response functions translate the sensitivity of a sensor head to its environment. It can be noted here that whatever the potential applied to the GRs, the general shape of the response function of the sensor head is very similar. However, an intensification of the GEF in the low deposited energies, when the GRs are floating, can be observed.

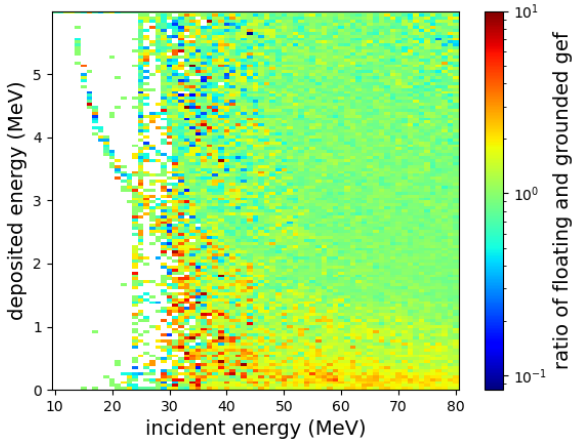

Fig. 9. Ratio of the proton RFs when the GRs are floating and grounded

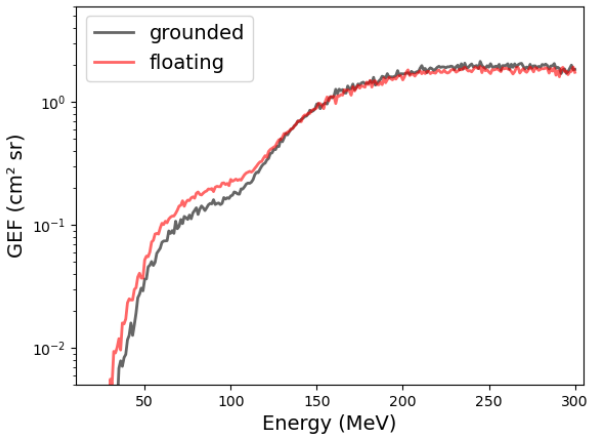

Fig. 10. Cuts of the proton RFs in the 500 keV – 800 keV deposited energy region. Grounded (black curve) and floating (red curve) cases are considered.

Fig. 10 shows two horizontal cross-sections of the floating and grounded PE1 RF. The observed deposited energies are relatively low and are in the 500 keV – 800 keV energy range. In the case where the guard rings are floating, Fig. 10 highlights the increase of the GEF for the low incident proton energies (up to ~100 MeV). This observation can be critical because the analysis of the response functions to deduce the fluxes of high energy protons is then more difficult. Indeed, high energy protons are mainly associated with low deposited energy. Thus, the information relative to high-energy protons is essentially located in the first few exploitable channels of the radiation monitor.

To estimate the loss of performance of the radiation monitor in the situation shown in Fig. 10, the bowtie technique can be applied, as described in [4], [20]. The general idea of this technique is to find the optimal parameters (e.g. cutoff energy for integrated fluxes) from a flux database and a RF. The flux database used here is built from the AP8 model [21]. Using the geometric factors as plotted in Fig. 10 for a cutoff energy of 120 MeV, the error obtained is 28% when the GRs are grounded and 64% when the GRs are floating. For higher cutoff energies, the errors are larger and the errors associated with floating GRs are systematically at least 2 times larger than those associated with grounded GRs.

Thus, having floating GRs degrades the performance of the radiation monitor to deduce the fluxes of high energy protons.

VII. Response functions using GRs as active shielding

GRs can be used to improve the performance of the radiation monitor. The case of the PE1 head currently embedded on E7C is used to estimate the potential improvements that can be provided by a non-conventional use of guard rings. However, this approach is not exploited for the mission and cannot be exploited because the required acquisition chain is not implemented.

In this mission, the PE1 detector head allows for the observation of protons from 60 MeV to 120 MeV with a good confidence level, as described in [4].

In the results presented in Fig. 11 and Fig. 12, the use of a 50 µm GR as active shielding is simulated. Passive shielding consists of the placement of intermediate material that can slow down or completely stop some particles. No additional measurements are performed on the added materials. On the other hand, active shielding is based on the exploitation of additional but limited information. In the approach proposed in [22], scintillators are used to evaluate the passage of a particle. Only a binary state is monitored with a comparison of the output current (scintillator + SiPM) against a threshold. A very similar approach is proposed here but using the currents collected on the GRs. This means that an additional acquisition chain (charge amplifier, shaper, etc.) is required.
Fig. 11 shows the current RF of the PE1 head on E7C (with a slightly smaller junction in order to integrate the GR) and the response function built with an "active" guard ring (see Fig. 12). With the addition of a guard ring, two new measurement modes are possible: coincidence (two or more sensitive regions are crossed by the same particle) and anticoincidence (only one of several sensitive regions is crossed by a particle). Thus, during the simulations, the anticoincidence mode corresponds to events where energy is deposited in the SSD and no current is measured on the GR.

Unlike the usual constructions of detection heads doing coincidence and anticoincidence modes, there are no stacked SSDs here.

Fig. 12 presents the RF of the PE1 head using the anticoincidence mode between the main junction and the GR. A large improvement can be observed on the response function, i.e., the first channels (associated with low deposited energies) are much cleaner. Thus, this response function would allow for the observation of protons of very high energies (up to about 250 MeV) with a very good confidence level.

As in the previous section, the bowtie technique can be used to quantify the benefit of Fig. 12 compared to Fig. 11. Let us consider the channels covering the deposited energies between 500 keV and 800 keV, and let us set the cutoff energy to 250 MeV. Without using the GR to create an anticoincidence mode (see Fig. 11), the error is 85%. By using the GR to

create an anticoincidence mode (see Fig. 12), the error drops considerably to only 16%.

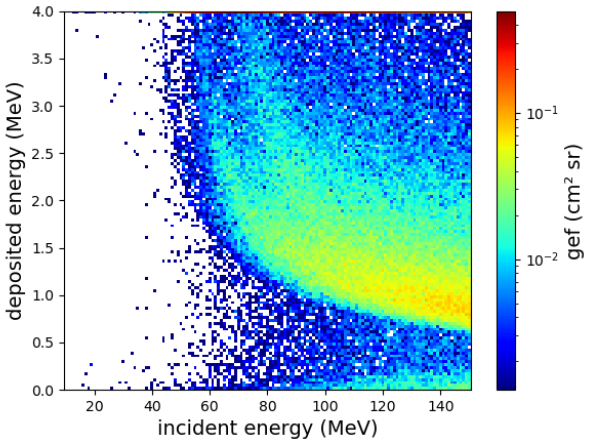

Fig. 11. Proton response function in single mode (mode currently in operation on E7C)

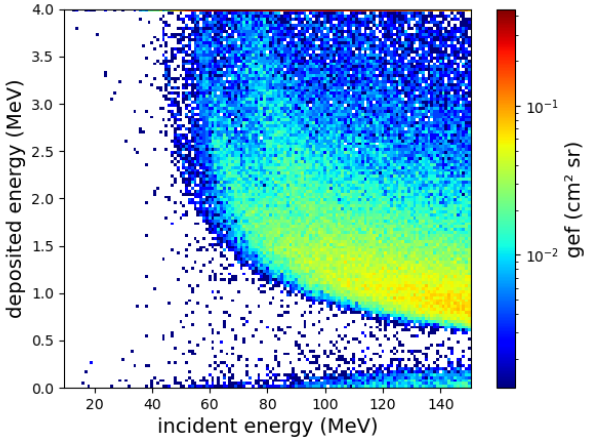

Fig. 12. Proton response function in anticoincidence mode (SSD + GRs)

VIII. Discussion

Floating GR or MGR in SSDs-based radiation monitors involves a potential degradation of the response functions. This is especially true considering that the main objective of the detection head is to observe high energy protons. To be more precise, depending on the characteristics of the GRs, this can change the nature of the RF on the first channels.

However, when the detection head uses several stacked SSDs and only coincidence modes are exploited, then the biasing of the GRs does not change anything.

In the case of the PE1 head (which is also valid for any detection head based on a single SSD), measuring the current of the guard rings extends the performance of the instrument. This is especially true for the measurement of particles that deposit a low quantity of energy (e.g. high energy protons)

IX. Conclusion

An analysis on SSDs and, more specifically, on the potential role of the associated GR was conducted. In response with experimental observations, our simulations effectively demonstrate multiple charge collection regimes when the GRs are floating.

When the radiative environment is not controlled (typically, in the radiation belts), and the incident beam cannot be directed to the center of the SSDs, floating the GRs may degrade the response functions.

The interest of having very high breakdown voltages is limited by the constraints of satellite integration. Thus, in the context of ICARE, the use of GRs grounded is preferred.

However, the GRs can be exploited in a different way by observing the collected charges. By doing so, the GRs can be used as active shielding allowing new acquisition modes. An application on the PE1 detector head, embedded on the E7C satellite, has shown a significant gain on the monitor performance.

X. References

[1] P. Laurent, S. Celestin, V. Maget, P. Caron, and F. Trompier, “Use of Scintillators to Study the Earth from Ground to the Radiation Belts,” in *Plastic Scintillators*, vol. 140, 2021, pp. 509–539. doi: 10.1007/978-3-030-73488-6_14.

[2] L. Desorgher *et al.*, “The Next Generation Radiation Monitor-NGRM,” in *2013 IEEE Nuclear Science Symposium and Medical Imaging Conference (2013 NSS/MIC)*, Oct. 2013, pp. 2632–2637. doi: 10.1109/NSSMIC.2013.6829497.

[3] M. Cyamukungu *et al.*, “The Energetic Particle Telescope (EPT) on Board PROBA-V: Description of a New Science-Class Instrument for Particle Detection in Space,” *IEEE Trans. Nucl. Sci.*, vol. 61, no. 6, pp. 3667–3681, 2014, doi: 10.1109/TNS.2014.2361955.

[4] P. Caron *et al.*, “In-Flight Measurements of Radiation Environment Observed by Eutelsat 7C (Electric Orbit Raising Satellite),” *IEEE Trans. Nucl. Sci.*, vol. 69, no. 7, pp. 1527–1532, Jul. 2022, doi: 10.1109/TNS.2022.3158470.

[5] J. B. Blake *et al.*, “The Magnetic Electron Ion Spectrometer (MagEIS) Instruments Aboard the Radiation Belt Storm Probes (RBSP) Spacecraft,” *Space Sci. Rev.*, vol. 179, no. 1–4, pp. 383–421, Nov. 2013, doi: 10.1007/s11214-013-9991-8.

[6] D. Boscher *et al.*, “In-Flight Measurements of Radiation Environment on Board the Argentinean Satellite SAC-D,” *IEEE Trans. Nucl. Sci.*, vol. 61, no. 6, pp. 3395–3400, Dec. 2014, doi: 10.1109/TNS.2014.2365212.

[7] D. Boscher *et al.*, “In Flight Measurements of Radiation Environment on Board the French Satellite JASON-2,” *IEEE Trans. Nucl. Sci.*, vol. 58, no. 3, pp. 916–922, Jun. 2011, doi: 10.1109/TNS.2011.2106513.

[8] N. Egorov *et al.*, “Operation of guard rings on the ohmic side of n+–p–p+ diodes,” *Nuclear Instruments and Methods in Physics Research Section A: Accelerators, Spectrometers, Detectors and Associated Equipment*, vol. 426, no. 1, pp. 197–205, Apr. 1999, doi: 10.1016/S0168-9002(98)01492-2.

[9] L. Evensen, A. Hanneborg, B. S. Avset, and M. Nese, “Guard ring design for high voltage operation of silicon detectors,” *Nucl. Instrum. Methods Phys. Res. Sect. Accel. Spectrometers Detect. Assoc. Equip.*, vol. 337, no. 1, pp. 44–52, Dec. 1993, doi: 10.1016/0168-9002(93)91136-B.

[10] V. Mishra, V. D. Srivastava, and S. K. Kataria, “Role of guard rings in improving the performance of silicon detectors,”

Pramana, vol. 65, no. 2, pp. 259–272, Aug. 2005, doi: 10.1007/BF02898614.

[11] J. Allison *et al.*, "Geant4 developments and applications," *IEEE Trans. Nucl. Sci.*, vol. 53, no. 1, pp. 270–278, Feb. 2006, doi: 10.1109/TNS.2006.869826.

[12] S. Agostinelli *et al.*, "Geant4—a simulation toolkit," *Nucl. Instrum. Methods Phys. Res. Sect. Accel. Spectrometers Detect. Assoc. Equip.*, vol. 506, no. 3, pp. 250–303, Jul. 2003, doi: 10.1016/S0168-9002(03)01368-8.

[13] J. Allison *et al.*, "Recent developments in Geant4," *Nucl. Instrum. Methods Phys. Res. Sect. Accel. Spectrometers Detect. Assoc. Equip.*, vol. 835, pp. 186–225, Nov. 2016, doi: 10.1016/j.nima.2016.06.125.

[14] H. Schindler and R. Veenhof, *Garfield++ — simulation of ionisation based tracking detectors*. [Online]. Available: http://garfieldpp.web.cern.ch/garfieldpp/

[15] W. Shockley, "Currents to Conductors Induced by a Moving Point Charge," *J. Appl. Phys.*, vol. 9, no. 10, pp. 635–636, Oct. 1938, doi: 10.1063/1.1710367.

[16] S. Ramo, "Currents Induced by Electron Motion," *Proc. IRE*, vol. 27, no. 9, pp. 584–585, Sep. 1939, doi: 10.1109/JRPROC.1939.228757.

[17] H. Schindler and R. Veenhof, "Garfield++ - UserGuide." Accessed: Apr. 02, 2022. [Online]. Available: https://garfieldpp.web.cern.ch/documentation/UserGuide.pdf

[18] D. Pfeiffer *et al.*, "Interfacing Geant4, Garfield++ and Degrad for the Simulation of Gaseous Detectors," *Nucl. Instrum. Methods Phys. Res. Sect. Accel. Spectrometers Detect. Assoc. Equip.*, vol. 935, pp. 121–134, Aug. 2019, doi: 10.1016/j.nima.2019.04.110.

[19] Synopsys, *Synopsys Sentaurus TCAD*. [Online]. Available: https://www.synopsys.com/

[20] A. Boudouridis, J. V. Rodriguez, B. T. Kress, B. K. Dichter, and T. G. Onsager, "Development of a Bowtie Inversion Technique for Real-Time Processing of the GOES-16/-17 SEISS MPS-HI Electron Channels," *Space Weather*, vol. 18, no. 4, art. no. e2019SW002403, Apr. 2020, doi: 10.1029/2019SW002403.

[21] D. M. Sawyer and J. I. Vette, *AP-8 trapped proton environment for solar maximum and solar minimum*. National Space Science Data Center (NSSDC), World Data Center A for Rockets and Satellites (WDC-A-R&S), 1976.

[22] M. Pinson, P. Caron, P. Laurent, and I. Cojocari, "Development of a Plastic Scintillator-Based Active Shield for the ICARE-NG Radiation Monitor," *IEEE Trans. Nucl. Sci.*, vol. 69, no. 7, pp. 1667–1674, Jul. 2022, doi: 10.1109/TNS.2022.3180555.